

Antiferromagnetic structure and electronic properties of BaCr_2As_2 and BaCrFeAs_2

Kai A. Filsinger,¹ Walter Schnelle,¹ Peter Adler,¹ Gerhard H. Fecher,¹ Manfred Reehuis,² Andreas Hoser,² Jens-Uwe Hoffmann,² Peter Werner,³ Martha Greenblatt,⁴ and Claudia Felser¹

¹*Max Planck Institute for Chemical Physics of Solids, Nöthnitzer Straße 40, 01187 Dresden, Germany*

²*Helmholtz-Zentrum Berlin für Materialien und Energie, 14109 Berlin, Germany*

³*Max Planck Institute of Microstructure Physics, Weinberg 2, 06120 Halle (Saale), Germany*

⁴*Department of Chemistry and Chemical Biology, Rutgers University, Piscataway, NJ, USA*

(Dated: January 13, 2017)

The chromium arsenides BaCr_2As_2 and BaCrFeAs_2 with ThCr_2Si_2 type structure (space group $I4/mmm$; also adopted by ‘122’ iron arsenide superconductors) have been suggested as mother compounds for possible new superconductors. DFT-based calculations of the electronic structure evidence metallic antiferromagnetic ground states for both compounds. By powder neutron diffraction we confirm for BaCr_2As_2 a robust ordering in the antiferromagnetic G -type structure at $T_N = 580$ K with $\mu_{\text{Cr}} = 1.9 \mu_B$ at $T = 2$ K. Anomalies in the lattice parameters point to magneto-structural coupling effects. In BaCrFeAs_2 the Cr and Fe atoms randomly occupy the transition-metal site and G -type order is found below 265 K with $\mu_{\text{Cr/Fe}} = 1.1 \mu_B$. ^{57}Fe Mössbauer spectroscopy demonstrates that only a small ordered moment is associated with the Fe atoms, in agreement with electronic structure calculations with $\mu_{\text{Fe}} \sim 0$. The temperature dependence of the hyperfine field does not follow that of the total moments. Both compounds are metallic but show large enhancements of the linear specific heat coefficient γ with respect to the band structure values. The metallic state and the electrical transport in BaCrFeAs_2 is dominated by the atomic disorder of Cr and Fe and partial magnetic disorder of Fe. Our results indicate that Néel-type order is unfavorable for the Fe moments and thus it is destabilized with increasing iron content.

I. INTRODUCTION

The discovery of high- T_c superconductivity in iron-based pnictides and chalcogenides has initiated intense efforts to investigate and theoretically model the magnetic states adopted by the non-superconducting relatives of these compounds [1–3]. Similar as for the oxocuprate superconductors, there is a subtle interplay between magnetism and superconductivity, and spin-fluctuations are considered as the mechanism enabling the formation of Cooper pairs [4]. The possible coexistence of specific types (spin-density wave, SDW) of magnetic order and superconductivity on the microscale in the Fe-based systems is an ongoing topic of research.

The antiferromagnetic (afm) parent compounds of cuprate superconductors are Mott (charge transfer) insulators. The situation is less clear for their Fe-based counterparts. For instance, non-superconducting pnictides like LaOFeAs or BaFe_2As_2 are metallic, itinerant antiferromagnets with low ordered moments at the iron sites ($< 1 \mu_B$), whereas chalcogenides like $\text{K}_{0.8}\text{Fe}_{1.6}\text{Se}_2$ are insulators with large Fe moments of $\approx 3 \mu_B$. Strictly, however, half-filled systems with d^5 configuration have to be regarded as the Mott-type parent compounds, which is confirmed by the semiconducting properties of e.g. BaMn_2As_2 [5–9] as well as of LaOMnAs and LiMnAs [10 and 11].

There is an ongoing debate about the proper description of the electronic structure of Fe-based pnictides and chalcogenides, in particular about the importance of electron correlation and the degree of electron itinerancy [12 and 13]. Since the basic Fe-As layers with formally Fe^{2+} ions in the parent compounds constitute a multi-

orbital system, orbital ordering is also believed to be of importance. Two opposing views have been adopted: On the one hand, the iron pnictides have been considered as weakly correlated metals where a SDW magnetic state is formed due to Fermi surface nesting. On the other hand, in particular the more strongly correlated selenides have been discussed as Mott-type insulators and the magnetism was modeled in terms of Heisenberg-type exchange interactions between localized moments. However, none of the limiting views can describe the many facets of magnetism which have emerged from experimental studies and actually it is believed that the Fe-based pnictides and chalcogenides are in between these extremes. For instance, even itinerant electronic systems may show pronounced correlation effects arising from Hund’s rule coupling (Hund’s metals [3 and 14]), which rationalizes the existence of large magnetic moments on short timescales of the order of femtoseconds, as derived from photoemission experiments [13].

An important prototype system is BaFe_2As_2 which adopts the tetragonal ThCr_2Si_2 -type crystal structure at room temperature and features a concomitant structural and magnetic transition at $T_N = 132$ K [15]. Below T_N a stripe-like afm order occurs with saturated Fe moments of about $0.9 \mu_B$ being aligned along the a axis of the low-temperature orthorhombic crystal structure [16]. BaFe_2As_2 can be converted into a high- T_c superconductor by hole or electron doping [15, 17, and 18] or by high pressure [19]. While substitution of Fe by some transition metals like Co, Ni or even Ru [20–22] induces superconductivity, substitution by others like Mn does not lead to superconducting states [23]. In contrast to BaFe_2As_2 , the half-filled Mn-analogue BaMn_2As_2 remains tetrago-

nal down to low temperatures and adopts a G -type afm spin structure with a high ordered moment ($3.9\mu_B$) and a high ordering temperature of 625 K [7 and 8]. Similarly high Néel temperatures (692–758 K) and G -type afm have been observed for the Cr species in the isostructural silicides RCr_2Si_2 ($R = Tb, Ho, Er$) [24].

Superconductivity in manganese and chromium compounds is very rare and only recently representatives have been found. The first, binary CrAs, has been long known for its structural and helimagnetic ordering transition at 240–190 K with sizable Cr moments of $1.67\mu_B$ [25]. The ordering temperature decreases dramatically to zero for pressures of 0.7–0.8 GPa and superconductivity with critical temperature up to 2.2 K appears [26 and 27]. At ambient pressure superconductivity has been investigated in the new $A_2Cr_3As_2$ ($A = K, Rb, Cs$) compounds featuring quasi onedimensional Cr_3As_3 tubes [28 and 29].

The Mott scenario for the transition-metal arsenides [30] considers a mirror-symmetry in the many-body physics arising when the half-filled d^5 configuration is either doped by electrons or by holes. The Cr compounds formally have a d^4 configuration and in this sense are the hole-doped analogues to the electron-doped d^6 system $BaFe_2As_2$. Recently, some theoretical studies explored the possibilities to find superconductivity for BaM_2As_2 and LaOMAs with transition-metals M (or mixtures) with less than 5 electrons [31 and 32]. Emphasis in these works is put on the strength of correlations in dependence of the band filling. It is hoped that correlations similar to those in the actual iron-based high T_c materials lead to superconductivity.

Here, we focus on the system $Ba(Fe_{1-x}Cr_x)_2As_2$, where no superconducting compositions have been found so far [23, 33, and 34]. Theoretical calculations predicted an afm checkerboard (G -type) ordering in the end member $BaCr_2As_2$ [35] and a ferromagnetic (fm) ground state in atomically ordered $BaCrFeAs_2$ [7]. Another electronic structure calculation predicted ordered $BaCrFeAs_2$ as a fully compensated antiferromagnet with an iron moment of $2.6\mu_B$ [36]. Such a material could be relevant for spintronics applications. Neutron diffraction studies on iron-rich $BaFe_{2-x}Cr_xAs_2$ single crystals with $0 < x < 0.94$ indicated that near $x = 0.6$ the SDW ground state is replaced by a G -type afm state [34], but spin structure and ordering temperature of the end member $BaCr_2As_2$ have not been studied experimentally yet. Also electronic structure calculations of $EuCr_2As_2$ suggested a stable G -type afm order of the Cr sublattice (in addition, the Eu^{2+} ions show fm ordering below 21 K) [37]. A recent experimental study confirmed these predictions [38].

We investigated the detailed crystal and magnetic structures of $BaCr_2As_2$ and $BaCrFeAs_2$ by temperature dependent powder neutron diffraction. Magnetic susceptibility, electrical transport, specific heat, and ^{57}Fe Mössbauer spectroscopy measurements complement the study. Our theoretical studies predict a random occupation of Cr and Fe on the transition-metal site for $BaCrFeAs_2$ and metallic afm G -type ordered ground

states for both compounds. Experimentally, it is shown that both compounds in fact feature G -type afm order, where the Néel temperature $T_N = 580$ K of $BaCr_2As_2$ is nearly as high as that of $BaMn_2As_2$, although the magnetic moment is only half as large. Both compounds are metallic conductors. $BaCrFeAs_2$ turns out to be atomically disordered, and thus only average magnetic moments are obtained from neutron diffraction. Most interestingly, the Fe Mössbauer spectra indicate that the Fe magnetic moments are much smaller than those of Cr and of similar size as in $BaFe_2As_2$. T_N decreases with increasing iron content, thus the G -type order is unfavorable for the Fe moments. The itinerant character of the magnetism persists in the whole stability range of the G -type order, whereas $BaMn_2As_2$ with the same nominal d electron count as $BaCrFeAs_2$ is a semiconductor.

II. EXPERIMENTAL & CALCULATION DETAILS

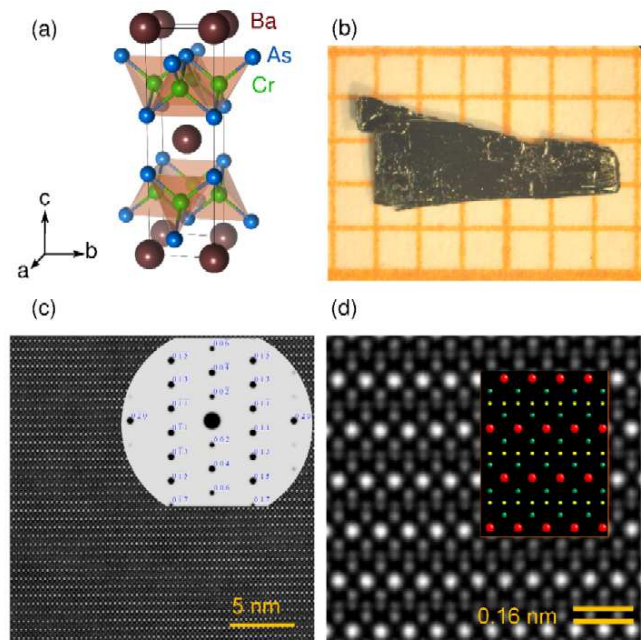


FIG. 1. a.) $BaCr_2As_2$ crystallizes in the $ThCr_2Si_2$ structure (space group $I4/mmm$). b.) Crystals form as shiny black platelets. c.) HAADF image and diffraction pattern. d.) Zoom of the HAADF image, the inset shows the theoretical atom positions (Ba red, Cr green, As yellow).

$BaCr_2As_2$ and $BaCrFeAs_2$ were synthesized by reacting CrAs and FeAs with Ba in an alumina crucible. The binaries were synthesized according to Singh *et al.* [35] using Cr (chemPUR, 99.99%), Fe (chemPUR, 99.9%), and As (Alfa Aesar, 99.999%). To control the harsh reaction between the binaries and Ba (Alfa Aesar, 99.999%), only 1/3 of the barium was added initially. The mixture was heated to 1423 K and held for 12 h. Then the prod-

uct was ground and additional Ba was added. These steps were repeated until the powder x-ray diffraction pattern (PXRD) did not show any CrAs or FeAs impurities. In both cases an excess of $\approx 5\%$ Ba was added to react all of the strongly magnetic CrAs or FeAs. Single crystals were grown using the Bridgman technique with alumina crucibles under argon atmosphere. The crucible was heated to 1823 K and held for 24 h, then it was moved with 1 mm h^{-1} out of the hot zone of the furnace. Single crystals (Figure 1b) up to $10 \times 5 \times 4 \text{ mm}$ could be grown. For the neutron diffraction experiments $\approx 4 \text{ g}$ of polycrystalline sample was prepared.

The crystal structure (ThCr₂Si₂ type, *tI10*, space group (SG) *I4/mmm*, No. 139, Ba on *2a*, Cr on *4d*, As on *4e*) was confirmed by PXRD using Cu-K α radiation ($\lambda = 1.54056 \text{ \AA}$), with a Huber G670 camera (Guinier technique). The refined lattice parameters are $a = 3.9667$ and $c = 13.6214 \text{ \AA}$ for BaCr₂As₂ and $a = 3.986$ and $c = 13.2939 \text{ \AA}$ for BaCrFeAs₂. Additional reflexes suggest the presence of traces of BaAl₂O₄ in some samples. High-resolution transmission electron microscopy (HR-TEM) microstructure studies were performed using a FEI Titan 80-300. In the high-angle annular dark field (HAADF) images (shown in Figures 1c and d for BaCr₂As₂; not shown for BaCrFeAs₂) no signs of disorder on the Ba *2a*(0,0,0), Cr/(CrFe) *4d* ($\frac{1}{2}, \frac{1}{2}, \frac{1}{2}$) or As *4e* (0,0,*z*) sites could be found. In agreement with the PXRD pattern, segregates of BaAl₂O₄ were seen on the surface for some BaCrFeAs₂ crystals. The average composition of the crystals was found to be Ba_{1.03(4)}Cr_{2.01(5)}As_{2.03(5)} and Ba_{1.01(6)}Cr_{0.96(8)}Fe_{1.08(2)}As_{2.10(1)} by chemical analysis with inductively coupled plasma optical emission spectroscopy (ICP-OES).

Powder neutron diffraction experiments on BaCr₂As₂ and BaCrFeAs₂ have been carried out on the instruments E2, E6, and E9 at the BER II reactor of the Helmholtz-Zentrum Berlin. The instrument E9 uses a Ge-monochromator selecting the neutron wavelength $\lambda = 1.7973 \text{ \AA}$, while the instruments E2 and E6 use a pyrolytic graphite monochromator selecting the neutron wavelength $\lambda = 2.38 \text{ \AA}$ and 2.42 \AA , respectively. On these instruments powder patterns were recorded in the following ranges of diffraction angles: $7.7^\circ \leq 2\theta \leq 83.4^\circ$ (E2), $7.5^\circ \leq 2\theta \leq 136.5^\circ$ (E6), and $8^\circ \leq 2\theta \leq 141^\circ$ (E9). In case of BaCr₂As₂ powder patterns were collected between 2 and 750 K, for BaCrFeAs₂ between 2 and 275 K. The refinements of the crystal and magnetic structure were carried out with FullProf [39] using the nuclear scattering lengths $b(\text{O}) = 5.805 \text{ fm}$, $b(\text{Cr}) = 3.635 \text{ fm}$, $b(\text{Fe}) = 9.54 \text{ fm}$, $b(\text{Ba}) = 5.25 \text{ fm}$ [40]. The magnetic form factors of the Cr³⁺ and Fe³⁺ ions were taken from Ref. 41.

Magnetization was measured in two magnetometer systems (MPMS-XL7 and MPMS3, Quantum Design). Only small differences were seen between data taken in warming after zero-field cooling (zfc) and during cooling in field (fc). For some crystals such differences seem to be due to tiny CrAs precipitations (see below). For one BaCr₂As₂ crystal the oven option of the MPMS3 was

employed. For these measurements the crystal was first measured at low temperatures and then cemented to a heater stick for the high-temperature run. The electrical resistivity, transverse magnetoresistance, Hall effect, and heat capacity were determined with a measurement system (ACT and HC options, respectively, PMMS9, Quantum Design) between 1.8 and 320 K.

Temperature-dependent Mössbauer spectra of BaCrFeAs₂ were measured with a standard WissEl spectrometer and a Janis closed cycle refrigerator (SHI-850-5) using a ⁵⁷Co/Rh source and a drive system operating in constant acceleration mode. The Mössbauer absorber consisted of an acrylic glass sample container with a sample density of $\approx 17 \text{ mg per cm}^2$. In order to ensure homogeneous distribution the sample was mixed with boron nitride. Spectra were collected between 5 and 292 K and evaluated with MossWinn [42]. Hyperfine field distributions were extracted using the Hesse-Rübartsch method. Isomer shifts are given relative to α -iron.

The electronic structures were calculated self-consistently in the local spin density approximation (LSDA) using the full potential linearized augmented plane wave (FLAPW) method including spin-orbit (SO) interaction as implemented in WIEN2k [43–45]. For atomically disordered BaCrFeAs₂ the calculations were carried out using the full potential, spin polarized relativistic Korringa-Kohn-Rostocker method (SPRKKR) [46 and 47]. All calculations were performed using the PBE exchange-correlation functional [48] and the generalized gradient approximation (GGA). To estimate the influence of a static correlation, the LDA+*U* method was applied.

For BaCr₂As₂ the calculations were started with the values $a = 3.96$, $c = 13.6 \text{ \AA}$, and $z = 0.361$ [49]. A *G*-type afm order was assumed and the lattice was set up in SG *I4m2* (119) and the Cr atoms were located on the split *2c* and *2d* sites to allow for the anti-parallel orientations of their magnetization. This space group concerns the atomic positions, the final magnetic symmetry depends on the direction of the quantization axis and is described by a Shubnikov color group (here *P 4'/m'm'm* (123.344)). A full structural optimization showed that the above given parameters are nearly relaxed, in agreement with previous observations [35].

In the calculations of the electronic structure for BaCrFeAs₂ the same basic atomic and magnetic structures were used. Two cases were assumed, an ordered and an alloyed structure. In the ordered structure, the initial *4d* position of the Cr atom was split and half of the new positions was occupied by Fe. This results in SG *I42m* (119) with Ba *2a*, Cr *2c*, Fe *2d*, and As *4e*. Starting from the experimental lattice parameters, an optimization of the ordered structure resulted in $a_{\text{opt}} = 4.012 \text{ \AA}$, $c_{\text{opt}} = 13.3819 \text{ \AA}$, and $z_{\text{opt}} = 0.357$. The strong deviations of these optimized parameters from the experimental ones suggest that the ordered case is not realized, i. e. in the actual material Cr and Fe are disordered. For the

TABLE I. Results of the crystal structure refinements for BaCr_2As_2 and BaCrFeAs_2 . Powder neutron diffraction data were collected at $T = 2\text{K}$ on the instrument E9. The refinements of the data sets were carried out in the tetragonal space group $I4/mmm$. The isotropic temperature factors of the different atoms were constrained to be equal.

BaCr ₂ As ₂ at 2 K, $R_N = 0.0480$					
$a = 3.9503(2)\text{ \AA}$, $c = 13.6047(10)\text{ \AA}$, $Z = 2$, $V = 212.30(3)\text{ \AA}^3$					
atom site	x	y	z	$B (\text{\AA}^2)$	
Ba	$2a$	0	0	0.32(3)	
Cr	$4d$	$0\frac{1}{2}$	$\frac{1}{4}$	0.32(3)	
As	$4e$	0	0.36092(14)	0.32(3)	
BaCrFeAs ₂ at 2 K, $R_N = 0.0402$					
$a = 3.9793(1)\text{ \AA}$, $c = 13.2532(4)\text{ \AA}$, $Z = 2$, $V = 209.86(1)\text{ \AA}^3$					
atom site	x	y	z	$B (\text{\AA}^2)$	
Ba	$2a$	0	0	0.19(2)	
Cr	$4d$	$0\frac{1}{2}$	$\frac{1}{4}$	0.19(2)	
Fe	$4d$	$0\frac{1}{2}$	$\frac{1}{4}$	0.19(2)	
As	$4e$	0	0.35779(10)	0.19(2)	

alloyed structure it was assumed that Fe and Cr occupy both the $2c$ and $2d$ position in a 50:50 ratio.

III. RESULTS

A. Crystal structures

The crystal structures of BaCr_2As_2 and BaCrFeAs_2 were investigated by powder neutron diffraction. Note that below $T_N = 580\text{K}$, respectively 265K , the patterns also included magnetic Bragg intensity (see Section III E). Both compounds crystallize in the tetragonal SG $I4/mmm$ (No. 139), where the Ba, Cr(Fe), and As atoms occupy the Wyckoff positions $2a(0,0,0)$, $4d(0,\frac{1}{2},\frac{1}{4})$, $4e(0,0,z)$, respectively. The same SG was reported earlier for BaMn_2As_2 [6]. From the data sets collected on the fine-resolution powder diffractometer E9 we could not find any additional peak splitting indicating a lower crystal structure symmetry. The refinements of the crystal structure of BaCr_2As_2 from data sets recorded in the temperature range from 2 up to 750 K resulted in residuals between $R_N = 0.048$ and 0.088 [defined as $R_N = (\sum||F_{\text{obs}}| - |F_{\text{calc}}||)/\sum|F_{\text{obs}}|$]. These values are somewhat larger than expected. This can be ascribed to the fact, that the investigated sample contained an impurity, which could not be characterized so far (see Figure 2). Further, additional impurity peaks of the sample container were observed in the diffraction patterns using the high temperature furnace on E9. Nevertheless, the lattice parameters, as well as the positional parameters of BaCr_2As_2 could be refined with good accuracy. In the case of BaCrFeAs_2 the crystal structure was investigated in the temperature range between 2 and 275 K. Due to the higher purity of this sample the refinements resulted in smaller residuals between $R_N = 0.035$ and

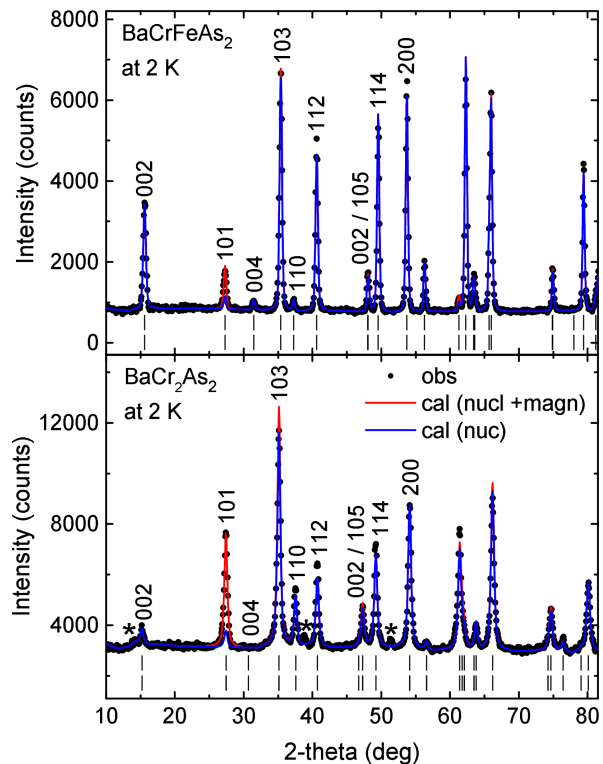


FIG. 2. Neutron diffraction patterns of BaCr_2As_2 and BaCrFeAs_2 powder taken at $T = 2\text{K}$. The calculated patterns of the pure nuclear contribution (blue) as well as the sum of the nuclear and the magnetic contribution (red) are compared with the observed ones (black full circles). In the lower part the positions of the Bragg peaks are given (black ticks). The BaCr_2As_2 sample contained an impurity (positions marked with *), which could not be identified so far.

0.043. The results of the Rietveld refinements of the data sets collected at 2 K are given in Table I. It is emphasized that there are no indications of superstructure reflections which would point to atomic order of Cr and Fe atoms.

Figure 3a shows the temperature dependence of the cell parameters as well as the cell volume. For BaCrFeAs_2 the lattice parameters a and c show a continuous increase from 2 up to 275 K, which is above the magnetic ordering temperature $T_N = 265(5)\text{K}$. A similar trend was found for BaMn_2As_2 [6]. A continuous increase of a and b was also observed for BaCr_2As_2 but only in the range from 2 K up to about 300 K. Further heating up to 700 K leads to a decrease of the c parameter, while the increase of the a -parameter becomes somewhat more pronounced (see Figure 3). As a consequence, the ratio c/a decreases from 3.43 at 300 K to 3.34 at 750 K. The former value is in agreement with literature data [49]. These results indicate that the magnetic transition in BaCr_2As_2 is accompanied by subtle structural modifications, in contrast to BaMn_2As_2 [6]. The anomaly in the c parameter is reflected in the change of the distance between the arsenic atoms lying along the c direction. Namely, one observes a decrease of the distance $d(\text{As-As})$ between

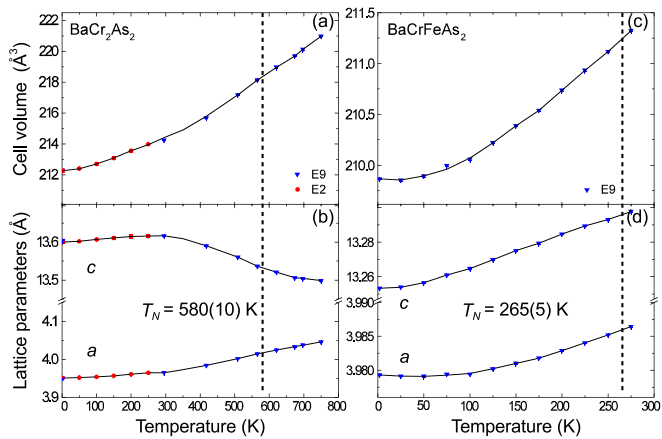


FIG. 3. Temperature dependence of the lattice parameters and the cell volumes of BaCr_2As_2 and BaCrFeAs_2 . These values were determined from data sets collected on the instruments E2 and E9.

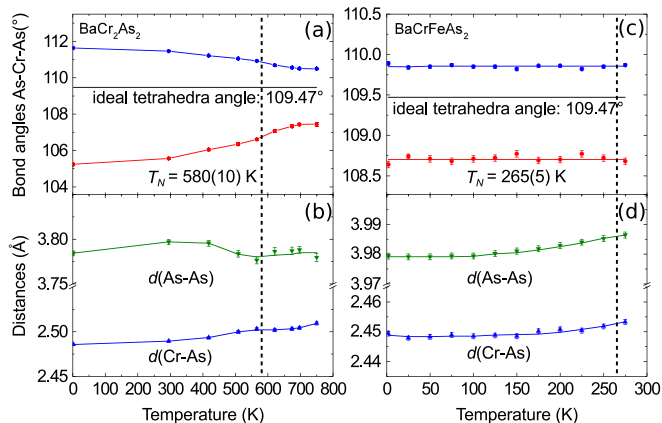


FIG. 4. Temperature dependence of the interatomic distances $d(\text{Cr-As})$ [$d(\text{Cr/Fe-As})$] and $d(\text{As-As})$ in BaCr_2As_2 and BaCrFeAs_2 . Also shown are the two bond angles $\angle_1(\text{As-Cr-As})$ (blue) and $\angle_2(\text{As-Cr-As})$ (red) in the CrAs_4 tetrahedron of BaCr_2As_2 and the corresponding angles for BaCrFeAs_2 .

about 300 K and the Néel temperature $T_N = 580(10)$ K as shown in Fig. 4. Above T_N finally $d(\text{As-As})$ seems to show a slight increase up to 750 K. The bond length $d(\text{Cr-As})$ only shows a slight increase from 2 K up to 750 K, but a weak anomaly is observed near T_N . On the other hand in BaCrFeAs_2 both, $d(\text{As-As})$ and $d(\text{Cr-As})$, only show a slight increase in the temperature range from 2 K and 275 K without anomalies, indicating that magnetic ordering does not influence the structural properties significantly. In Fig. 4 we have also plotted the changes of the two different bond angles $\angle_1(\text{As-Cr-As})$ and $\angle_2(\text{As-Cr-As})$ in the CrAs_4 (and Cr/FeAs_4) tetrahedra, which form a twodimensional layer in the ab plane. The structural anomalies accompanying the magnetic transition in BaCr_2As_2 are also reflected in the bond angles. Thus, the bond angles $\angle_1(\text{As-Cr-As})$ and $\angle_2(\text{As-Cr-As})$ show a strong increase and decrease in the magnetically ordered

state down to 2 K. Above 650 K both bond angles seem to reach saturation values. In contrast, the two bond angles for BaCrFeAs_2 are practically unchanged between 2 and 275 K. However, both pnictides do not reach the ideal tetrahedron angle of 109.47° . The CrAs_4 tetrahedra in BaCr_2As_2 are stronger distorted than the Cr/FeAs_4 tetrahedra in BaCrFeAs_2 .

B. Electronic structure of BaCr_2As_2

In Figure 5 the Fermi surface of BaCr_2As_2 is shown. Three bands are crossing the Fermi energy ϵ_F , resulting in three iso-surfaces. The innermost one is closed and has a cushion shape. It is related to a hole pocket around the Γ point. The outer two are open at top and bottom and have corrugated cylinder shapes with fourfold arranged bulges. The effective band mass m^*/m_e of the innermost hole pocket was determined for the Δ and Σ directions revealing values of $m_\Delta^* = -0.63$ and $m_\Sigma^* = -0.39$ at the Γ point. This hints that this band is in the GGA-LSDA not responsible for the observed enhanced value of the electronic specific heat coefficient γ (cf. Ref. 35 and our specific heat results in section III D).

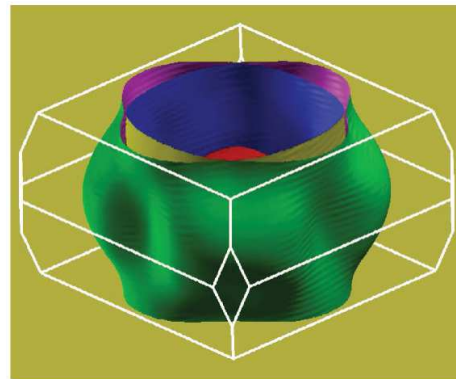


FIG. 5. Fermi surface of BaCr_2As_2 .

The evolution of the DOS with increasing Coulomb parameter U in the LDA+ U calculation is given in Figure 6. Note that the unoccupied minority states of one of the Cr atoms correspond to the unoccupied majority states of the other, and vice versa for the occupied states due to the anti-symmetric spin densities of an antiferromagnet. The increased U results in an increase of the magnetic moment at the Cr atoms (cf. Table II). Their values are in the range $2.4\text{-}3.5 \mu_B$.

The “bare” coefficient of the electron specific heat $\gamma_0 = \pi^2 k_B^2 n(\epsilon_F)/3$ for BaCr_2As_2 is $\approx 8 \text{ mJ mol}^{-1} \text{ K}^{-2}$. For the various calculation schemes the results are also given in Table II. The inclusion of SO interaction has only a weak effect on γ_0 . For LDA+ U , it is found that $n(\epsilon_F)$ – and thus γ_0 – increases slightly and has a maximum at $U \approx 1 \text{ eV}$, but then decreases with further increase of U . Using SPRKKR and the mean field approximation a Néel temperature $T_{N,\text{calc}} \approx 880 \text{ K}$ can be calculated.

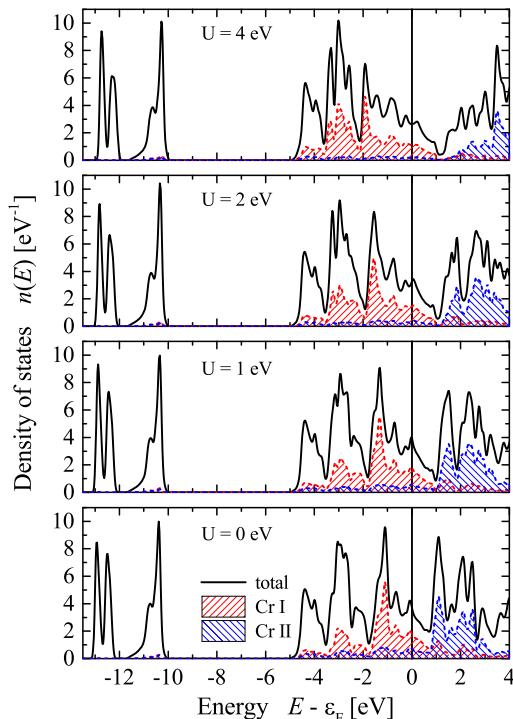


FIG. 6. Density of states of BaCr_2As_2 calculated with $\text{LDA}+U$. Shown is the total DOS together with the local DOS at Cr atoms for increasing U .

TABLE II. Spin magnetic moment of the Cr atoms, the DOS at the Fermi energy $n(\epsilon_F)$, and the coefficient of the electron specific heat γ_0 for different calculation schemes for G -type afm ordered BaCr_2As_2 . All calculations were performed including spin-orbit interaction (SO).

method	U eV	m_{Cr} μ_B	$n(\epsilon_F)$ eV^{-1}	γ_0 $\text{mJ mol}^{-1} \text{K}^{-2}$
GGA with SO	0	2.4	3.37	7.95
LDA+ U	1	2.8	3.67	8.65
	2	3.1	2.45	5.77
	3	3.3	2.91	6.85
	4	3.4	2.85	6.71
	5	3.5	1.84	4.35

C. Electronic structure of BaCrFeAs_2

The electronic structure of the ordered variant of BaCrFeAs_2 should be a completely compensated half-metallic ferromagnet as reported in Reference [36]. The peculiarity of this type of magnetism is that the moment of two different types of atoms – here Cr and Fe – compensate each other similar to an antiferromagnet. The different symmetry, however, allows that the DOS in the two spin channels are different. Moreover, a band gap at ϵ_F appears in one of the spin densities similar to a half-metallic ferromagnet. The DOS for the \uparrow spin channel has a pronounced maximum just above ϵ_F with a value of $n(\epsilon_F + \delta) = 6.92 \text{ eV}^{-1}$ ($\delta \approx 50 \text{ meV}$). This value is

twice as high as the one calculated for BaCr_2As_2 . It arises from flat bands around ϵ_F . A detailed analysis of the DOS reveals that those states are localized at the Fe atoms. In many cases, compounds with such a peaked DOS at ϵ_F are not stable.

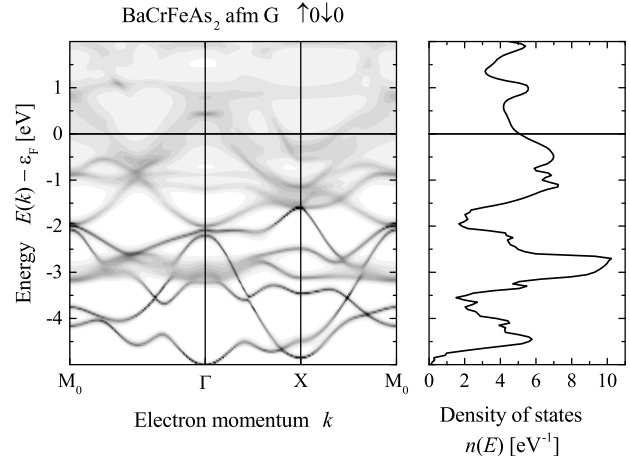


FIG. 7. Electronic structure of BaCrFeAs_2 with chemical disorder between Cr and Fe. Shown is the case with a vanishing magnetic moment at Fe. The DOS is the same in both spin channels due to the afm order, thus the sum is plotted.

The electronic structure and the DOS of the alloy variant of BaCrFeAs_2 are shown in Fig. 7. The result of the chemical disorder scattering are strongly broadened electronic states, in particular close to ϵ_F . The broadening causes a reduction of the maximum of the DOS just above ϵ_F to about 5 eV^{-1} , which is still higher compared to BaCr_2As_2 .

The magnetic properties of ordered and alloyed BaCrFeAs_2 are compared in Table III. The moment for the atomically ordered phase compares well with $2.6 \mu_B$ reported in Ref. 36. The moments in the ordered case are not completely the same, the vanishing total moment is guaranteed by the polarization of the interstitial and the atoms in the vicinity of the magnetic Cr and Fe atoms. The orbital magnetic moments are very small, in the order of $0.002 \mu_B$ or $0.06 \mu_B$.

Interestingly, for the random distribution of Fe and Cr, a stable solution is found with vanishing moments at the Fe atoms at the same site. The calculation was started with a starting moment at the Cr atoms ($4 \mu_B$) but zero moment at Fe. No magnetic moment was induced during the self consistent cycles. The result is an average moment of $1.38 \mu_B$ for the $2c/2d$ positions.

Also for BaCrFeAs_2 the Néel temperature can be calculated in the mean field approximation using SPRKKR. The value for the atomically ordered structure is very high, however, a much lower Néel temperature of about 260 K is obtained for the disordered version.

TABLE III. Magnetic properties of BaCrFeAs₂. Tabulated are the DOS just above ϵ_F (n_{\max}), the absolute values of the magnetic moments at Cr and Fe species ($m_{\text{Cr/Fe}}$), and the calculated Néel temperatures ($T_{\text{N,calc}}$).

	ordered	disordered	
n_{\max}	6.92	4.99	(eV ⁻¹)
m_{Cr}	2.74	2.76	(μ_B)
m_{Fe}	2.53	0.00	(μ_B)
$T_{\text{N,calc}}$	965	260	(K)

D. Magnetic and thermal properties, electrical transport

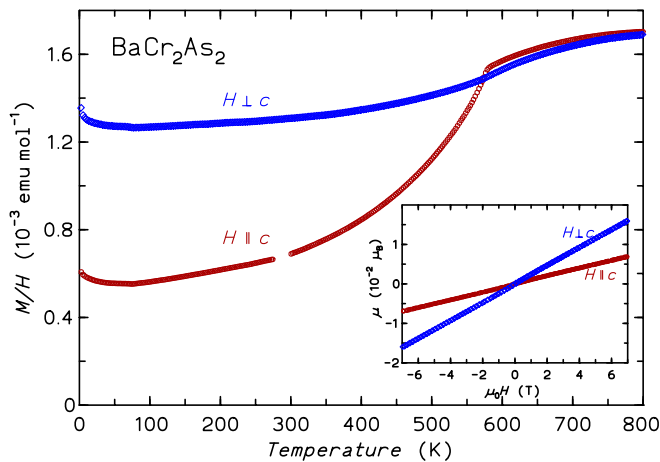


FIG. 8. Magnetic susceptibility of a BaCr₂As₂ crystal in a field $\mu_0 H = 1$ T perpendicular (blue diamonds) and parallel (red circles) to the crystallographic c axis. Minor adjustments of the magnetometer oven data sets ($T > 400$ K) were made to match with the data below 400 K. The inset shows the magnetic moment from an isothermal magnetization loop measured at a temperature $T = 1.8$ K.

The temperature dependence of the magnetic susceptibility, $\chi = M/H$, at $\mu_0 H = 1$ T of a BaCr₂As₂ crystal platelet (ab plane) was measured with the magnetic field parallel and perpendicular to the c axis (Fig. 8). The small difference between the directions above 600 K suggests a rather weak anisotropy in the paramagnetic regime. However, no Curie-Weiss behavior could be observed up to $T = 800$ K. For $H \parallel c$ a clear kink is visible, indicating the afm ordering of the Cr sub-lattice at $T_{\text{N}} = 575(10)$ K, as determined from the peak in the derivative $d(\chi T)/dT$. The decrease of $\chi(T)$ for $H \parallel c$ towards low temperatures is much stronger than for $H \perp c$, eventually suggesting an afm order with magnetic moments aligned along the c axis. The behavior of $\chi(T)$ and the ordering temperature is very similar to that of BaMn₂As₂ [8]. The nearly isotropic but non-Curie-Weiss behavior above T_{N} is observed for several afm compounds

with ThCr₂Si₂-type structure. It is typical for the somewhat twodimensional character of the magnetic interactions and has been treated in detail theoretically for BaMn₂As₂ [8]. For BaCr₂As₂ the smooth maximum of $\chi(T)$ may be anticipated for temperatures around 900 K.

A small upturn of $\chi(T)$ in both directions for temperatures below ≈ 50 K suggests the presence of paramagnetic impurities, e.g. from point defects. Magnetization loops taken at $T = 1.8$ K (Fig. 8 inset) show a very small fm-like component of $< 5 \times 10^{-4} \mu_B$ for both field along or perpendicular to the c axis. Also, in measurements of $M(T)$ at $\mu_0 H = 0.01$ T, a small sharp transition from a fm impurity phase becomes visible at $T_{\text{imp}} \approx 76$ K. We assign this transition and the fm-like signals to the structural and helimagnetic ordering transition of CrAs [25]. The ordering temperature of CrAs is known to decrease dramatically to zero for pressures of 0.7-0.8 GPa [26 and 27]. We speculate that CrAs on the crystal surface is strained and its ordering temperature is therefore reduced to T_{imp} .

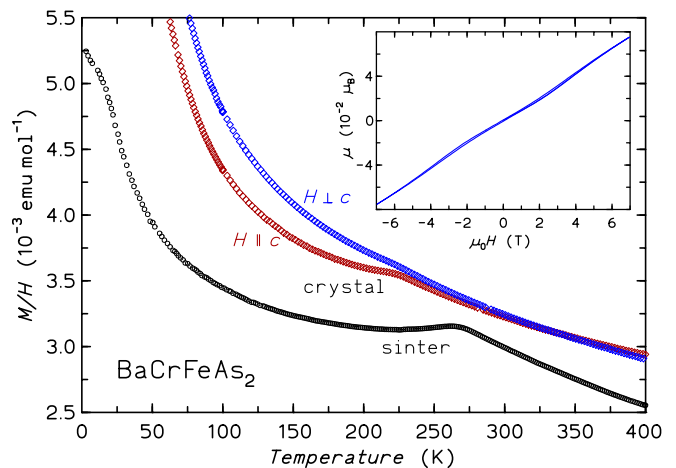


FIG. 9. Magnetic susceptibility of the BaCrFeAs₂ sintered sample used for the other measurements (black circles) in a field $\mu_0 H = 1$ T. For comparison, the susceptibility of a BaCrFeAs₂ crystal (diamonds) with field perpendicular and parallel to the c axis is shown (shifted up by 5×10^{-4} emu mol⁻¹). The crystal has a lower Néel temperature. The inset shows the magnetization loop at $T = 2.0$ K

The magnetic susceptibility of sintered BaCrFeAs₂ (Fig. 9) displays a broadened cusp at $T_{\text{N}} \approx 269(2)$ K (midpoint of step in $d(\chi T)/dT$), but there is only a slight decrease of the $\chi(T)$ curve below this temperature. Instead, with decreasing temperature the susceptibility increases again, indicating a strong paramagnetic contribution following a Curie law. Above the Néel temperature (range 300-400 K) the data are well fitted by a Curie-Weiss law with effective moment $\mu_{\text{eff}} = 3.70 \mu_B$ and Weiss temperature $\theta_P = -273$ K. The BaCrFeAs₂ crystal shows a similar cusp, however at ≈ 225 K. The lower T_{N} of the single crystal is probably due to a slightly lower Fe content compared to the sinter sample. The decrease of $\chi(T)$ is more pronounced for $H \parallel c$, suggesting an afm ordered

structure with the magnetic moments lying in the crystallographic c direction. The paramagnetic contribution in the magnetically ordered state of BaCrFeAs_2 is discussed in connection with the Mössbauer results (Sec. III F).

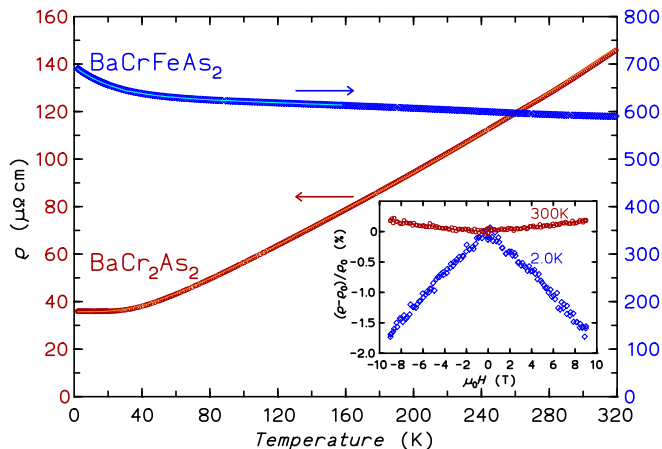


FIG. 10. Electrical resistivity of a BaCr_2As_2 crystal measured in the crystallographic ab plane (red circles) and of a sintered sample of BaCrFeAs_2 (blue diamonds) in zero magnetic field. The resistivity curves in $\mu_0 H = 9$ T (lines) almost coincide with the zero-field data. The inset shows the magnetoresistance $100 \times (\rho - \rho_0)/\rho_0$ as function of field for BaCr_2As_2 measured at $T = 2.0$ and 300 K.

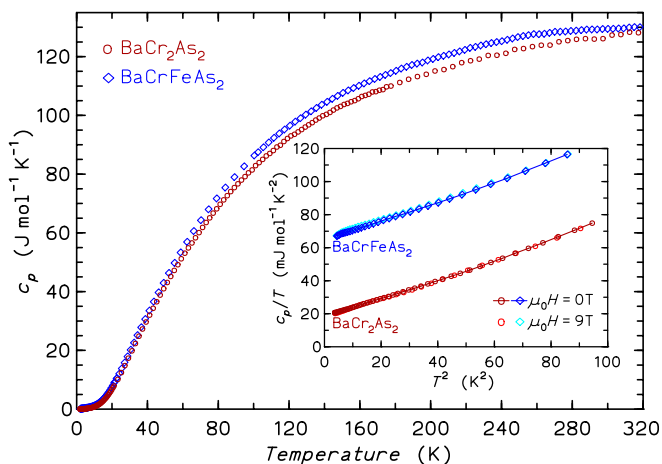


FIG. 11. Molar specific heat $c_p(T)$ of a BaCr_2As_2 single crystal (red circles) and of polycrystalline sintered BaCrFeAs_2 (blue diamonds). Inset: c_p/T vs. T^2 representation for low temperatures. Zero-field data (dark symbols and line) and data in a magnetic field $\mu_0 H = 9$ T (light symbols) are shown.

The electrical resistivity, $\rho(T)$, of the BaCr_2As_2 crystal measured for current in the ab plane (Fig. 10) increases almost linearly with temperature and indicates metallic behavior of the compound ($\rho_{300\text{K}} = 136 \mu\Omega \text{ cm}$). The residual resistance ratio $\text{RRR} \approx 3.8$ indicates a fair quality of the specimen and the residual resistance is already reached at ≈ 13 K. Interestingly, below this temperature

$\rho(T)$ increase very slightly (by $\approx 0.1\%$ of ρ_0). The magnetoresistance (MR, Fig. 10 inset) is very small and positive for high temperatures. Surprisingly, for $T = 2.0$ K it is negative and quite strong (-1.7% at $\mu_0 H = 9$ T). This might indicate the damping of an additional scattering mechanism at very low temperatures compared to the T_N . The origin of both the upturn of $\rho(T)$ below 13 K and of the negative MR might be due to a Kondo-hole effect. Non-magnetic atoms replacing magnetic Cr in the afm ordered lattice can give rise to a Kondo-like upturn of resistivity at low temperatures. This scattering is weakened by the application of a magnetic field resulting in a negative MR proportional to the field. The Hall resistivity curves $\rho_{ab}(H)$ are linear, the Hall constants are positive and do almost not vary with temperature. This observation is consistent with the hole pocket around the Γ point (cf. Fig. 5). Within a one-band model the Hall constant corresponds to a hole density $n_h \approx 1.5 \times 10^{22} \text{ cm}^{-3}$ and low mobility ($b_h = 11 \text{ cm}^2 \text{ V}^{-1} \text{ s}^{-1}$ at $T = 2$ K).

For polycrystalline BaCrFeAs_2 (Fig. 10) as well as for a single crystal (not shown) the electrical resistivity is about five times higher. Interestingly, it displays only a weak temperature dependence and increases continuously with decreasing temperature. Similar to BaCr_2As_2 there is an upturn below a certain temperature (here, ≈ 40 K). The absence of a typical metallic resistivity behavior is probably due to scattering of charge carriers on the disordered Cr/Fe species of the $4d$ Wyckoff site. The order of magnitude suggests however that BaCrFeAs_2 is still a metal. Nominally isoelectronic BaMn_2As_2 crystals grown in MnAs flux show an about 100 times higher resistivity [6]. The magnetoresistance of BaCrFeAs_2 is small ($< 0.15\%$) for all temperatures, indicating that magnetic scattering due to the atomic Cr/Fe disorder is unimportant. Also for BaCrFeAs_2 the Hall isotherms $\rho_{xy}(H)$ are linear, however Hall constants are negative and vary with temperature. They correspond to electron densities $n_e = 8.3 \times 10^{21} \text{ cm}^{-3}$ at $T = 300$ K and only $1.5 \times 10^{21} \text{ cm}^{-3}$ at 2 K with $b_e = 6 \text{ cm}^2 \text{ V}^{-1} \text{ s}^{-1}$.

The specific heat, $c_p(T)$, of the two compounds is presented in Fig. 11. For BaCr_2As_2 no anomalies from transitions are visible up to 320 K. However, $c_p(T)$ for BaCrFeAs_2 is larger than that of BaCr_2As_2 in the covered temperature range which might also be due to the Cr/Fe disorder. A very small steplike anomaly can be seen at ≈ 260 K (barely standing out of the noise). The transition temperature is in agreement with our magnetization and neutron diffraction data (see Section III E). The small entropy change connected with this magnetic ordering is due to the low ordered moments of Cr/Fe and the predominantly itinerant character of the magnetic system. The Dulong-Petit limit $c_p = 3nR$ ($R =$ molar gas constant, $n =$ number of atoms) is reached by both compounds at around room temperature.

At low temperatures the specific heats (see Fig. 11 inset) are well described by $c_p(T) = \gamma T + \beta T^3 + \delta T^5$ where γ is the coefficient of the linear term γT (usually assigned to conduction electrons) and βT^3 and δT^5 are the first

two terms due to the harmonic theory of lattice specific heat. For BaCr_2As_2 (BaCrFeAs_2) least-squares fits in the range 1.9–7 K result in $\gamma = 18.8$ (64.9) $\text{mJ mol}^{-1} \text{K}^{-1}$, $\beta = 0.51$ (0.56) $\text{mJ mol}^{-1} \text{K}^{-4}$ corresponding to an initial Debye temperature of 268 (259) K, and $\delta = 0.6$ (0.0) $\mu\text{J mol}^{-1} \text{K}^{-6}$. The γ value obtained for BaCr_2As_2 is close to the value deduced by Singh *et al.* [35], however the linear term of BaCrFeAs_2 is very large. The γ value for BaCrFeAs_2 is confirmed through measurements on the single crystal for which we show the susceptibility in Fig. 9. The lattice properties (Debye temperatures) of the two compounds are similar, as expected from the small atomic mass difference of Cr and Fe. Also, afm spin waves do not play a role due to the high Néel temperatures.

The linear specific heat contribution is insensitive to magnetic fields (cf. Fig. 11 inset). For BaCr_2As_2 in a field $\mu_0 H = 9 \text{ T}$ the linear coefficient γ is not changed at all. For BaCrFeAs_2 the specific heat increases slightly in $\mu_0 H = 9 \text{ T}$ for $T < 5 \text{ K}$ (by maximally 1.8% at 3.3 K), which might be due to a Schottky-type anomaly due to minor impurities. Thus, the enhanced γ values should either not be due to spin fluctuations at all or the spin fluctuations are of too high in energy. Especially BaCr_2As_2 has a very high Néel temperature and the fluctuations might not be quenchable by such a small field.

E. Magnetic structures

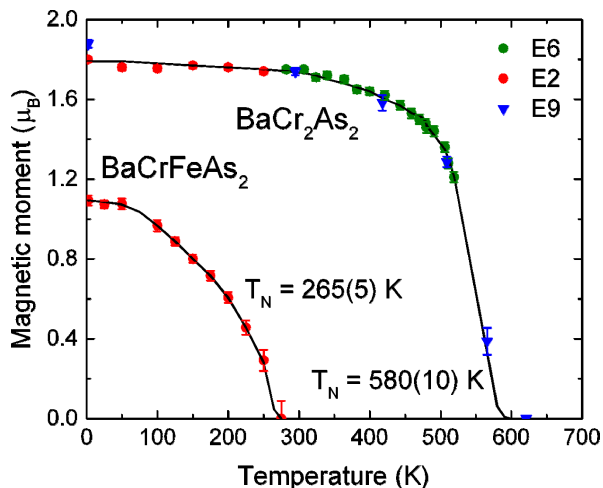


FIG. 12. Temperature dependence of the magnetic moments per transition-metal atom in BaCr_2As_2 and BaCrFeAs_2 as obtained from powder neutron diffraction data (instruments E2, E6, and E9). Magnetic intensity of Bragg reflections disappears at the Néel temperatures $T_N = 580(10) \text{ K}$ and $T_N = 265(5) \text{ K}$ respectively.

In order to investigate the magnetic structure of BaCr_2As_2 we have collected a powder neutron pattern at 2 K. In comparison to the data collected at 750 K, well above the Néel temperature $T_N = 580 \text{ K}$, it was

shown that magnetic intensities appear at the positions of nuclear Bragg reflections indicating a magnetic structure, which can be described with the propagation vector $\mathbf{k} = 0$. This shows that the translation $\mathbf{t} = (\frac{1}{2}, \frac{1}{2}, \frac{1}{2})$ associated with the I cell is not lost. In Figure 2 it can be seen that the strongest magnetic intensity is observed at $2\theta = 27.4^\circ$, which is the position of the Bragg reflection 101. Strong intensity could be generated at this position using a magnetic structure model, where the chromium atoms in the Wyckoff positions $4d$, located at $(0, \frac{1}{2}, \frac{1}{4})$ and $(\frac{1}{2}, 0, \frac{1}{4})$, are coupled antiparallel. Due to the I centering the operation $\mathbf{t} = (\frac{1}{2}, \frac{1}{2}, \frac{1}{2})$ does not change the direction of the spin. Therefore one finds the spin sequence $+-+-$ for the Cr atoms in the positions $(0, \frac{1}{2}, \frac{1}{4})$, $(\frac{1}{2}, 0, \frac{1}{4})$, $(\frac{1}{2}, 0, \frac{3}{4})$, and $(0, \frac{1}{2}, \frac{3}{4})$.

Using this structure model the magnetic structure could be successfully refined, when the magnetic moments are aligned parallel to the c axis. The same type of magnetic ordering is found for BaMn_2As_2 and also for the Cr sublattice in EuCr_2As_2 [38]. Assuming an additional magnetic component within the ab plane, magnetic intensity should appear at the position of the reflection 002. Magnetic intensity could not be easily determined from the difference patterns collected at 2 and 750 K, in the fully ordered and the paramagnetic state, because the strong structural changes lead to a change of the nuclear intensity of the reflection 002. Therefore we have refined simultaneously the crystal and the magnetic structure at 2 K. The calculated nuclear intensity of the 002 reflection is even slightly larger than the observed one. This clearly indicates the absence of an additional magnetic component within the ab plane, i. e. the absence of any spin canting to the c axis. From the data set collected at 2 K on instrument E9 we finally found for the Cr atoms a magnetic moment of $\mu_{\text{exp}} = 1.88(2)\mu_B$ resulting in a residual $R_M = 0.0268$ [defined as $R_M = (\sum ||I_{\text{obs}}| - |I_{\text{calc}}||) / \sum |I_{\text{obs}}|$]. From the data set collected on instrument E2 the magnetic moment $\mu_{\text{exp}} = 1.80(2)\mu_B$ was found to be slightly smaller (residual $R_M = 0.118$). It has to be mentioned that the moment value determined from the E9 data is more reliable, since the overall scale factor could be determined with higher accuracy (a much larger number of nuclear Bragg reflections was available). From the data collected on E2, E6, and E9 we are able to determine the temperature dependence of the magnetic moment up to the Néel temperature $T_N = 580(10) \text{ K}$ (see Figure 12). The results from the neutron diffraction experiments compare well with those from magnetization data of the BaCr_2As_2 single crystal (Fig. 8). The experimental magnetic Cr moments at 2 K compare reasonably well with the values obtained from our (cf. Table II and previous [35] electronic structure calculations. The experimental Cr moment is even slightly smaller than the calculated moments. This shows that electronic correlation effects reflected in the parameter U of the LDA+ U calculations do not play a role as increasing U lead to larger Cr magnetic moments.

Accordingly we have determined the magnetic struc-

ture of BaCrFeAs₂. As it can be seen in Figure 2 the strongest magnetic intensity could also be observed at the position of the reflection 101. The magnetic intensities of BaCrFeAs₂ are found to be much weaker than those in BaCr₂As₂ indicating that the averaged magnetic moments of the Cr and Fe atoms are strongly reduced. A moment $\mu_{\text{exp}} = 1.09(3)\mu_{\text{B}}$ was refined resulting in a residual $R_{\text{M}} = 0.068$. The Néel temperature $T_{\text{N}} = 265(5)$ K compares well with our magnetic susceptibility data (Fig. 9).

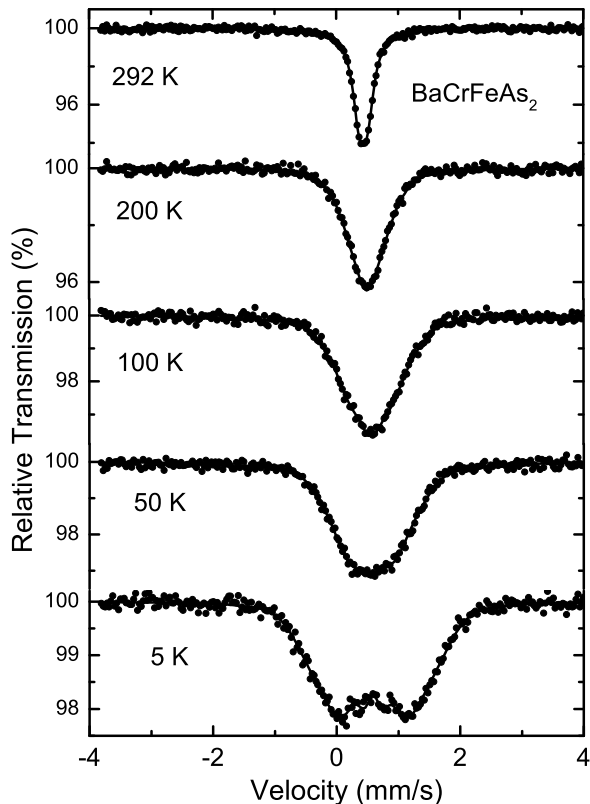


FIG. 13. Mössbauer spectra of BaCrFeAs₂ at the indicated temperatures. Dots correspond to the experimental data, solid lines to the best fits.

F. Mössbauer spectroscopy on BaCrFeAs₂

Representative ⁵⁷Fe Mössbauer spectra of BaCrFeAs₂ are shown in Figure 13. The room temperature spectrum appears as a broadened line which can be fitted by a quadrupole doublet with an isomer shift IS of 0.44 mm s^{-1} and a quadrupole splitting QS of 0.13 mm s^{-1} . By contrast, the spectrum at 5 K features a complex broad pattern which evidences the presence of magnetic hyperfine splitting. The spectrum was fitted by assuming a distribution of hyperfine fields, yielding $IS = 0.59 \text{ mm s}^{-1}$ and a peak hyperfine field $B_{\text{hf}} = 5.4 \text{ T}$. The isomer shifts are slightly larger than those of BaFe₂As₂ [50] which adopts the SDW phase below the magnetic order-

ing temperature. Nevertheless the local electronic structure is quite similar in the two compounds. Most remarkably, the peak B_{hf} of about 5 T in BaCrFeAs₂ is nearly the same as the B_{hf} in the magnetically ordered phases of BaFe₂As₂ [50] and LaOFeAs [51]. From the neutron diffraction study we obtained an average magnetic moment of $1.09 \mu_{\text{B}}$ per magnetic ion. Assuming that the Cr moment is the same as in BaCr₂As₂ ($1.8 \mu_{\text{B}}$) we estimate the iron moment as $0.4 \mu_{\text{B}}$.

It has been pointed out that a direct estimation of Fe moments from B_{hf} is questionable due to spin-orbit induced contributions to B_{hf} in the iron pnictides [52]. Nevertheless, a small iron moment is in qualitative agreement with the small B_{hf} for BaCrFeAs₂. A similarly small iron moment of $0.4 \mu_{\text{B}}$ was reported for LaOFeAs [53], whereas a larger moment of $0.9 \mu_{\text{B}}$ was derived for BaFe₂As₂ [16]. The spectra of BaCrFeAs₂ are, however, much less resolved than those of BaFe₂As₂ and LaOFeAs which reflects the Fe-Cr disorder in the present material giving rise to a broad B_{hf} distribution. Both, neutron diffraction and Mössbauer data confirm that Fe and Cr atoms are disordered, while some previous electronic structure calculations assumed an ordered arrangement [6 and 36]. A large ordered Fe moment of $2.5\text{--}2.6 \mu_{\text{B}}$ predicted from the electronic structure calculations for atomically ordered BaCrFeAs₂ (Ref. 36 and Table III) is incompatible with the neutron diffraction and the Mössbauer data.

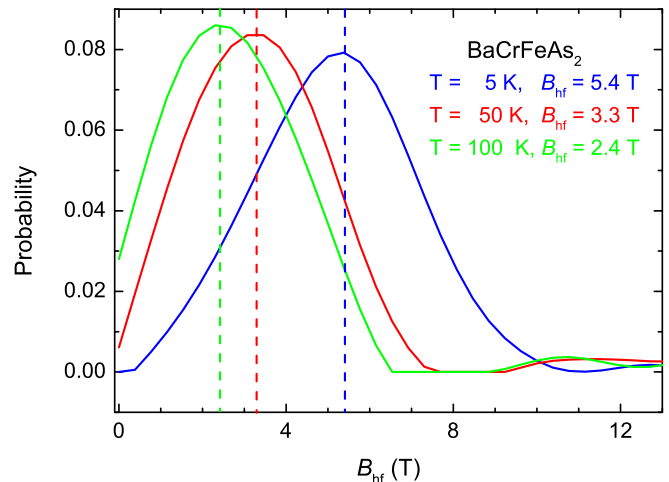


FIG. 14. Hyperfine field distributions in the low-temperature range which were extracted from Mössbauer spectra of BaCrFeAs₂. The dashed lines indicate the positions of the peak hyperfine fields given in the Figure.

Indications for an unusual behavior of the Fe moments is obtained from the temperature dependence of B_{hf} . With increasing temperature a pronounced decrease in hyperfine splitting is apparent even in the temperature region 5–100 K (Figure 13), which is unexpected as the Néel temperature is much higher (265 K). At 100 K the B_{hf} distribution even extends down to 0 T (Figure 14) indicating that a fraction of the iron atoms is already

non-magnetic. These observations are in contrast to the behavior of BaFe_2As_2 where in this temperature range only a minor reduction of B_{hf} was observed although T_{N} is considerably smaller (≈ 140 K) [50]. The strong decrease of the peak B_{hf} from 5.4 T at 5 K to 2.4 T at 100 K is also in sharp contrast to the temperature dependence of the total magnetic moments derived from neutron diffraction (Figure 12).

A possible scenario is that the Fe moments do not participate in the G -type afm structure and rather freeze in the low temperature range which is consistent with the fact that no anomaly is apparent in the temperature dependence of the moments between 2 and 100 K. The formation of the G -type afm order then is still driven by the large Cr moments. Further on, the upturn in the susceptibility $\chi(T)$ below $T_{\text{N}} = 265$ K (Fig. 9), which is in contrast to the behavior of BaCr_2As_2 , is a further indication that the iron moments are at least partially disordered. As demonstrated above electronic structure calculations of atomically disordered BaCrFeAs_2 starting with zero Fe moment result in a stable solution with $\mu_{\text{Fe}} \sim 0$ and $\mu_{\text{Cr}} = 2.76 \mu_{\text{B}}$. The resulting average moment of $1.38 \mu_{\text{B}}$ per formula unit of BaCrFeAs_2 is not too far from the experimental moment of $1.09 \mu_{\text{B}}$. The mismatch of the Fe moments with G -type antiferromagnetism explains why T_{N} in Fe-substituted BaCr_2As_2 decreases drastically from 580 K in the parent compound to ≈ 50 K for an iron content of about 70 % where finally the G -type order becomes unstable and is replaced by the SDW structure [34]. At higher temperature the hyperfine splitting further decreases and for $T \geq 200$ K essentially a broad unstructured line is found. In this temperature range the Fe atoms are possibly polarized by the Cr moments. Above 260 K only minor changes in line broadening occur which compares well with $T_{\text{N}} = 265$ K obtained from neutron diffraction and susceptibility data.

IV. CONCLUSIONS

We have studied in detail the structural, electronic, and magnetic properties of BaCr_2As_2 and BaCrFeAs_2 . BaCr_2As_2 as well as LaOCrAs [31 and 32] have been discussed recently in connection with the Mott scenario (see Section I) of transition-metal arsenide superconductivity. Our powder neutron diffraction studies verify that BaCr_2As_2 adopts the theoretically predicted G -type afm order at $T_{\text{N}} = 580$ K and an ordered moment $\mu_{\text{Cr}} = 1.9 \mu_{\text{B}}$ at 2 K. Evidence for magneto-structural coupling effects was found and it remains to be clarified whether this reflects some type of electronic instability. The experimental magnetic Cr moment agrees well with LDA electronic structure calculations whereas incorporation of electron correlation within the LDA+ U scheme leads to Cr moments which are too high. T_{N} is 1/3 lower than the ordering temperature calculated within mean-field approximation, underlining the somewhat twodimensional character of the magnetic system.

BaCrFeAs_2 still adopts this G -type afm structure but the ordering temperature is less than half of that of BaCr_2As_2 . The small average moment $\mu_{\text{Cr/Fe}} \approx 1.1 \mu_{\text{B}}$ in connection with the small hyperfine field from Mössbauer spectra is in agreement with the results of our calculations for atomically disordered BaCrFeAs_2 and an Fe moment $\mu_{\text{Fe}} \sim 0$. The Néel temperature calculated within mean-field approximation is in good agreement with the experimental value (260 K and 265 K, respectively). Also the average Cr/Fe moment is in fair agreement with the calculation ($2.76 \mu_{\text{B}}$, distributed on two atoms). These findings, together with an anomalous temperature dependence of the hyperfine field, indicate that the small Fe moments are not incorporated into the G -type afm order. Thus it may be conjectured that Fe favors the stripe-type and Cr the checkerboard-type spin fluctuations, the latter being considered to be detrimental to superconductivity [4]. In case of electron pairing mediated by spin-fluctuations this finding would be in agreement with the fact that so far no superconductivity was observed for BaCr_2As_2 or Cr-substituted BaFe_2As_2 . Similarly, no superconductivity was found in Mn-substituted BaFe_2As_2 , where the pure Mn compound BaMn_2As_2 adopts a stable G -type afm order as well. Accordingly not only the doping level but also the type of spin fluctuations has to be considered for predictions of new superconducting compositions.

Both BaCr_2As_2 and BaCrFeAs_2 are metals. The linear specific heat (Sommerfeld) coefficients γ are much larger than expected from band theory, by a factor of 2.4 for BaCr_2As_2 and a huge factor of 5.5 for BaCrFeAs_2 . The discrepancies for both compounds cannot be resolved by reasonable strengths of correlations. However it seems that for BaCrFeAs_2 the disorder of the magnetic Cr and Fe atoms to some extent additionally boosts the γ value.

Our findings may be compared with results for the better investigated Mn 122 system. In contrast to BaCr_2As_2 BaMn_2As_2 is semiconducting [5–9]. The nominal $3d^5$ compound has a Néel temperature which is slightly higher than that of BaCr_2As_2 . It is possible to induce a metallic state in BaMn_2As_2 by application of pressure [54] or by hole-doping with as little as 1.6 % of K [55]. In this metallic state $\text{Ba}_{1-x}\text{K}_x\text{Mn}_2\text{As}_2$ is still G -type ordered [56] and is thus similar to BaCr_2As_2 . But there is one important difference, the Sommerfeld γ in the metallic Mn system is much smaller ($8.4 \text{ mJ mol}^{-1} \text{ K}^{-1}$ for $x = 0.05$ [55]) than in BaCr_2As_2 . This suggests that electronic correlations are weak in the BaMn_2As_2 materials. A recent photoemission (ARPES) study corroborates that there is almost no band renormalization with respect to the DFT-based band structure in BaMn_2As_2 [9]. An ARPES study on BaCr_2As_2 would therefore be highly welcome in order to shed more light on the development of electronic correlations in the 122 family of transition-metal arsenides.

For $\text{Ba}_{1-x}\text{K}_x\text{Mn}_2\text{As}_2$ the Néel temperature and the ordered Mn moment remain almost constant up to high substitution levels ($x \leq 0.4$) [56]. In contrast, in

the substitution series $\text{BaFe}_{2-x}\text{Mn}_x\text{As}_2$ for a low Mn substitution level $x = 0.15$ a clear competition between stripe-type and checkerboard-type spin fluctuations could be observed by inelastic neutron scattering [57], quite similar to the $\text{BaCr}_{2-x}\text{Fe}_x\text{As}_2$ series [34]. For $\text{BaFe}_{2-x}\text{Mn}_x\text{As}_2$ a miscibility gap prevents the synthesis of single-phase material for Mn contents $x > 0.24$ [58].

Although both modified BaMn_2As_2 -based ($3d^5$) materials [54–56] as well as BaCr_2As_2 are afm-ordered metals, until now there are no ways known to obtain superconductors based on these materials. The partial substitution of Ba by K in BaCr_2As_2 (hole doping) showed to be unsuccessful, but surprisingly resulted in the discovery of superconducting $\text{K}_2\text{Cr}_3\text{As}_3$ [28 and 29]. Another way

to possibly generate superconductivity in Mn or Cr-based 122 or 1111-type arsenides is the application of high pressure. With high pressure, in transition-metal arsenides structural instabilities come into play. We have now undertaken a structural and electrical transport study on one of our BaCr_2As_2 crystals under high pressure, the results of which will be reported elsewhere [59].

ACKNOWLEDGMENTS

We thank Ralf Koban for assistance and Igor Veremchuk for spark plasma sintering of a sample. MG acknowledges support of nsf-dmr 1507252 grant.

-
- ¹ E. Bascones, B. Valenzuela, and M. J. Calderón, Magnetic interactions in iron superconductors: A review, *Comptes Rendus Phys.* **17**, 36 (2016), URL <https://doi.org/10.1016/j.crhy.2015.05.004>.
- ² P. Dai, Antiferromagnetic order and spin dynamics in iron-based superconductors, *Rev. Modern Phys.* **87**, 855 (2015), URL <https://doi.org/10.1103/RevModPhys.87.855>.
- ³ Q. Si, R. Yu, and E. Abrahams, High temperature superconductivity in iron pnictides and chalcogenides, *Nature Reviews Materials* **1**, 16017 (2016), URL <https://doi.org/10.1038/natrevmats.2016.17>.
- ⁴ R. M. Fernandes and A. J. Millis, Suppression of superconductivity by Néel-type magnetic fluctuations in the iron pnictides, *Phys. Rev. Lett.* **110**, 117004 (2013), URL <https://doi.org/10.1103/PhysRevLett.110.117004>.
- ⁵ J. An, A. S. Sefat, D. J. Singh, and M.-H. Du, Electronic structure and magnetism in BaMn_2As_2 and BaMn_2Sb_2 , *Phys. Rev. B* **79**, 075120 (2009), URL <https://doi.org/10.1103/PhysRevB.79.075120>.
- ⁶ Y. Singh, A. Ellern, and D. C. Johnston, Magnetic, transport, and thermal properties of single crystals of the layered arsenide BaMn_2As_2 , *Phys. Rev. B* **79**, 094519 (2009), URL <https://doi.org/10.1103/PhysRevB.79.094519>.
- ⁷ Y. Singh, M. A. Green, Q. Huang, A. Kreyssig, R. J. McQueeney, D. C. Johnston, and A. I. Goldman, Magnetic order in BaMn_2As_2 from neutron diffraction measurements, *Phys. Rev. B* **80**, 100403 (2009), URL <https://doi.org/10.1103/PhysRevB.80.100403>.
- ⁸ D. C. Johnston, R. J. McQueeney, B. Lake, A. Honecker, M. E. Zhitomirsky, R. Nath, Y. Furukawa, V. P. Antropov, and Y. Singh, Magnetic exchange interactions in BaMn_2As_2 : A case study of the $J_1 - J_2 - J_c$ Heisenberg model, *Phys. Rev. B* **84**, 094445 (2011), URL <https://doi.org/10.1103/PhysRevB.84.094445>.
- ⁹ W.-L. Zhang et al., Angle-resolved photoemission observation of Mn-pnictide hybridization and negligible band structure renormalization in BaMn_2As_2 and BaMn_2Sb_2 , *Phys. Rev. B* **94**, 155155 (2016), URL <https://doi.org/10.1103/PhysRevB.94.155155>.
- ¹⁰ A. Beleanu et al., Large resistivity change and phase transition in the antiferromagnetic semiconductors LiMnAs and LaOMnAs , *Phys. Rev. B* **88**, 184429 (2013), URL <https://doi.org/10.1103/PhysRevB.88.184429>.
- ¹¹ S. Dong, W. Li, X. Huang, and E. Dagotto, First principles study of the magnetic properties of LaOMnAs , *J. Appl. Phys.* **115**, 17D723 (2014), URL <https://doi.org/10.1063/1.4867757>.
- ¹² P. Dai, J. Hu, and E. Dagotto, Magnetism and its microscopic origin in iron-based high-temperature superconductors, *Nature Phys.* **8**, 709 (2012), URL <https://doi.org/10.1038/nphys2438>.
- ¹³ N. Mannella, The magnetic moment enigma in Fe-based high temperature superconductors, *J. Phys.: Condens. Matter* **26**, 473202 (2014), URL <https://doi.org/10.1088/0953-8984/26/47/473202>.
- ¹⁴ S. Backes, H. O. Jeschke, and R. Valenti, Microscopic nature of correlations in multiorbital AFe_2As_2 ($A = \text{K}, \text{Rb}, \text{Cs}$): Hund’s coupling versus Coulomb repulsion, *Phys. Rev. B* **92**, 195128 (2015), URL <https://doi.org/10.1103/PhysRevB.92.195128>.
- ¹⁵ M. Rotter, M. Tegel, D. Johrendt, I. Schellenberg, W. Hermes, and R. Pöttgen, Spin-density-wave anomaly at 140 K in the ternary iron arsenide BaFe_2As_2 , *Phys. Rev. B* **78**, 020503 (2008), URL <https://doi.org/10.1103/PhysRevB.78.020503>.
- ¹⁶ Q. Huang, Y. Qiu, W. Bao, M. A. Green, J. W. Lynn, Y. C. Gasparovic, T. Wu, G. Wu, and X. H. Chen, Neutron-diffraction measurements of magnetic order and a structural transition in the parent BaFe_2As_2 compound of FeAs-based high-temperature superconductors, *Phys. Rev. Lett.* **101**, 257003 (2008), URL <https://doi.org/10.1103/PhysRevLett.101.257003>.
- ¹⁷ G.-F. Chen, Z. Li, G. Li, W.-Z. Hu, J. Dong, J. Zhou, X.-D. Zhang, P. Zheng, N.-L. Wang, and J.-L. Luo, Superconductivity in hole-doped $(\text{Sr}_{1-x}\text{K}_x)\text{Fe}_2\text{As}_2$, *Chinese Phys. Lett.* **25**, 3403 (2008).
- ¹⁸ K. Sasmal, B. Lv, B. Lorenz, A. M. Guloy, F. Chen, Y.-Y. Xue, and C.-W. Chu, Superconducting Fe-based compounds $(\text{A}_{1-x}\text{Sr}_x\text{Fe}_2\text{As}_2$ with $A = \text{K}$ and Cs with transition temperatures up to 37 K, *Phys. Rev. Lett.* **101**, 107007 (2008), URL <https://doi.org/10.1103/PhysRevLett.101.107007>.
- ¹⁹ P. L. Alireza, Y. T. C. Ko, J. Gillett, C. M. Petrone, J. M. Cole, G. G. Lonzarich, and S. E. Sebastian, Superconductivity up to 29 K in SrFe_2As_2 and BaFe_2As_2 at high pressures, *J. Phys.: Condens. Matter* **21**, 012208 (2008), URL <https://doi.org/10.1088/0953-8984/21/1/012208>.

- ²⁰ A. S. Sefat, R. Jin, M. A. McGuire, B. C. Sales, D. J. Singh, and D. Mandrus, Superconductivity at 22 K in Co-doped BaFe_2As_2 crystals, *Phys. Rev. Lett.* **101**, 117004 (2008), URL <https://doi.org/10.1103/PhysRevLett.101.117004>.
- ²¹ A. Leithe-Jasper, W. Schnelle, C. Geibel, and H. Rosner, Superconducting state in $\text{SrFe}_{2-x}\text{Co}_x\text{As}_2$ by internal doping of the iron arsenide layers, *Phys. Rev. Lett.* **101**, 207004 (2008), URL <https://doi.org/10.1103/PhysRevLett.101.207004>.
- ²² W. Schnelle, A. Leithe-Jasper, R. Gumeniuk, U. Burkhardt, D. Kasinathan, and H. Rosner, Substitution-induced superconductivity in $\text{SrFe}_{2-x}\text{Ru}_x\text{As}_2$ ($0 \leq x \leq 2$), *Phys. Rev. B* **79**, 214516 (2009), URL <https://doi.org/10.1103/PhysRevB.79.214516>.
- ²³ D. Kasinathan, A. Ormeci, K. Koch, U. Burkhardt, W. Schnelle, A. Leithe-Jasper, and H. Rosner, AFe_2As_2 ($A = \text{Ca, Sr, Ba, Eu}$) and $\text{SrFe}_{2-x}\text{TM}_x\text{As}_2$ ($\text{TM} = \text{Mn, Co, Ni}$): crystal structure, charge doping, magnetism and superconductivity, *New J. Phys.* **11**, 025023 (2009), URL <https://doi.org/10.1088/1367-2630/11/2/025023>.
- ²⁴ O. Moze, M. Hofmann, J. M. Cadogan, K. H. J. Buschow, and D. H. Ryan, Magnetic order in RCr_2Si_2 intermetallics, *Eur. Phys. J. B-Condens. Matter and Complex Systems* **36**, 511 (2003), URL <https://doi.org/10.1140/epjb/e2004-00006-4>.
- ²⁵ H. Boller and A. Kallel, First order crystallographic and magnetic phase transition in CrAs, *Solid State Commun.* **9**, 1699 (1971).
- ²⁶ W. Wu, J. Cheng, K. Matsubayashi, P. Kong, F. Lin, C. Jin, N. Wang, Y. Uwatoko, and J. Luo, Superconductivity in the vicinity of antiferromagnetic order in CrAs, *Nature Commun.* **5**, 5508 (2014), URL <https://doi.org/10.1038/ncomms6508>.
- ²⁷ H. Kotegawa, S. Nakahara, H. Tou, and H. Sugawara, Superconductivity of 2.2 K under pressure in helimagnet CrAs, *J. Phys. Soc. Japan* **83**, 093702 (2014), URL <https://doi.org/10.7566/JPSJ.83.093702>.
- ²⁸ J.-K. Bao, J.-Y. Liu, C.-W. Ma, Z.-H. Meng, Z.-T. Tang, Y.-L. Sun, H.-F. Zhai, H. Jiang, H. Bai, C.-M. Feng, Z.-A. Xu, and G.-H. Cao, Superconductivity in quasi-one-dimensional $\text{K}_2\text{Cr}_3\text{As}_3$ with significant electron correlations, *PRX* **5**, 011013 (2015), URL <https://doi.org/10.1103/PhysRevX.5.011013>.
- ²⁹ G.-H. Cao, J.-K. Bao, Z.-T. Tang, Y. Liu, and H. Jiang, Peculiar properties of Cr_3As_3 -chain-based superconductors (2016), arXiv:1609.09635.
- ³⁰ H. Ishida and A. Liebsch, Fermi-liquid, non-Fermi-liquid, and Mott phases in iron pnictides and cuprates, *Phys. Rev. B* **81**, 054513 (2010), URL <https://doi.org/10.1103/PhysRevB.81.054513>.
- ³¹ M. Edelmann, G. Sangiovanni, M. Capone, and L. de'Medici, Chromium analogues of iron-based superconductors (2016), arXiv:1610.10054.
- ³² J. M. Pizarro, M. J. Calderon, J. Liu, M. M. noz, and E. Bascones, Strong correlations and the search for high- T_c superconductivity in chromium pnictides and chalcogenides (2016), arXiv:1610.09560.
- ³³ A. S. Sefat, D. J. Singh, L. H. VanBebber, Y. Mozharivskyj, M. A. McGuire, R. Jin, B. C. Sales, V. Keppens, and D. Mandrus, Absence of superconductivity in hole-doped $\text{BaFe}_{2-x}\text{Cr}_x\text{As}_2$ single crystals, *Phys. Rev. B* **79**, 224524 (2009), URL <https://doi.org/10.1103/PhysRevB.79.224524>.
- ³⁴ K. Marty, A. D. Christianson, C. H. Wang, M. Matsuda, H. Cao, L. H. VanBebber, J. L. Zarestky, D. J. Singh, A. S. Sefat, and M. D. Lumsden, Competing magnetic ground states in nonsuperconducting $\text{Ba}(\text{Fe}_{1-x}\text{Cr}_x)_2\text{As}_2$ as seen via neutron diffraction, *Phys. Rev. B* **83**, 060509 (2011), URL <https://doi.org/10.1103/PhysRevB.83.060509>.
- ³⁵ D. J. Singh, A. S. Sefat, M. A. McGuire, B. C. Sales, D. Mandrus, L. H. VanBebber, and V. Keppens, Itinerant antiferromagnetism in BaCr_2As_2 : Experimental characterization and electronic structure calculations, *Phys. Rev. B* **79**, 094429R (2009), URL <https://doi.org/10.1103/PhysRevB.79.094429>.
- ³⁶ S.-J. Hu and X. Hu, Half-metallic antiferromagnet BaCrFeAs_2 , *J. Phys. Chem. C* **114**, 11614 (2010).
- ³⁷ U. B. Paramanik, R. Prasad, C. Geibel, and Z. Hossain, Itinerant and local-moment magnetism in EuCr_2As_2 single crystals, *Phys. Rev. B* **89**, 144423 (2014), URL <https://doi.org/10.1103/PhysRevB.89.144423>.
- ³⁸ S. Nandi, Y. Xiao, N. Qureshi, U. B. Paramanik, W. T. Jin, Y. Su, B. Ouladdiaf, Z. Hossain, and T. Brückel, Magnetic structures of the Eu and Cr moments in EuCr_2As_2 : Neutron diffraction study, *Phys. Rev. B* **94**, 094411 (2016), URL <https://doi.org/10.1103/PhysRevB.94.094411>.
- ³⁹ J. Rodríguez-Carvajal, Recent advances in magnetic structure determination by neutron powder diffraction, *Physica B: Condens. Matter* **192**, 55 (1993).
- ⁴⁰ V. F. Sears, in *International Tables for Crystallography*, edited by A. J. C. Wilson (Kluwer Academic Publishers, Dordrecht/Boston/London, 1995), vol. C, p. 383.
- ⁴¹ P. J. Brown, in *International Tables for Crystallography*, edited by A. J. C. Wilson (Kluwer Academic Publishers, Dordrecht/Boston/London, 1995), vol. C, p. 391.
- ⁴² MossWinn 4.0. <http://mosswinn.com>.
- ⁴³ P. Blaha, K. Schwarz, P. Sorantin, and S. B. Trickey, *Comp. Phys. Comm.* **59**, 399 (1999).
- ⁴⁴ K. Schwarz and P. Blaha, *Comput. Mater. Sci.* **28**, 259 (2003).
- ⁴⁵ P. Blaha, K. Schwarz, G. K. H. Madsen, D. Kvasnicka, and J. Luitz, *WIEN2k, an augmented plane wave + local orbitals program for calculating crystal properties – revised edition 14.2* (Karlheinz Schwarz, Techn. Universitaet Wien, Wien, Austria, 2014).
- ⁴⁶ H. Ebert, in *Electronic Structure and Physical Properties of Solids. The Use of the LMTO Method*, edited by H. Dreyse (Springer-Verlag, Berlin, Heidelberg, 1999), vol. 535 of *Lecture Notes in Physics*, p. 191.
- ⁴⁷ H. Ebert, D. Ködderitzsch, and J. Minar, Calculating condensed matter properties using the KKR-Green's function method recent developments and applications, *Rep. Prog. Phys.* **74**, 096501 (2011), URL <http://stacks.iop.org/0034-4885/74/i=9/a=096501>.
- ⁴⁸ J. P. Perdew, K. Burke, and M. Ernzerhof, *Phys. Rev. Lett.* **77**, 3865 (1996), URL <https://doi.org/10.1103/PhysRevLett.77.3865>.
- ⁴⁹ M. Pfisterer and G. Nagorsen, Bindungsverhältnisse und magnetische Eigenschaften ternärer Arsenide ET_2As_2 , *Z. Naturforsch. B* **35b**, 703 (1980).
- ⁵⁰ A. Błachowski, K. Ruebenbauer, J. Żukrowski, K. Rogacki, Z. Bukowski, and J. Karpinski, Shape of spin density wave versus temperature in AFe_2As_2 ($A = \text{Ca, Ba, Eu}$): A Mössbauer study, *Phys. Rev. B* **83**, 134410 (2011), URL <https://doi.org/10.1103/PhysRevB.83.134410>.

- ⁵¹ M. A. McGuire, A. D. Christianson, A. S. Sefat, B. C. Sales, M. D. Lumsden, R. Jin, E. A. Payzant, D. Mandrus, Y. Luan, V. Keppens, V. Varadarajan, J. W. Brill, R. P. Hermann, M. T. Sougrati, F. Grandjean, and G. J. Long, Phase transitions in LaFeAsO: Structural, magnetic, elastic, and transport properties, heat capacity and Mössbauer spectra, *Phys. Rev. B* **78**, 094517 (2008), URL <https://doi.org/10.1103/PhysRevB.78.094517>.
- ⁵² G. Derondeau, J. Minár, and H. Ebert, Hyperfine fields in the BaFe₂As₂ family and their relation to the magnetic moment, *Phys. Rev. B* **94**, 214508 (2016), URL <https://doi.org/10.1103/PhysRevB.94.214508>.
- ⁵³ C. de la Cruz, Q. Huang, J. W. Lynn, J. Li, W. Ratcliff II, J. L. Zarestky, H. A. Mook, G. F. Chen, J. L. Luo, N. L. Wang, and P. Dai, Magnetic order close to superconductivity in the iron-based layered LaO_{1-x}F_xFeAs systems, *Nature* **453**, 899 (2008), URL <https://doi.org/10.1038/nature07057>.
- ⁵⁴ A. T. Satya, A. Mani, A. Arulraj, N. V. Chandrashekar, K. Vinod, C. S. Sundar, and A. Bharathi, Pressure-induced metallization of BaMn₂As₂, *Phys. Rev. B* **84**, 180515(R) (2011), URL <https://doi.org/10.1103/PhysRevB.84.180515>.
- ⁵⁵ A. Pandey, R. S. Dhaka, J. Lamsal, Y. Lee, V. K. Anand, A. Kreyssig, T. W. Heitmann, R. J. McQueeney, A. I. Goldman, B. N. Harmon, A. Kaminski, and D. C. Johnston, Ba_{1-x}K_xMn₂As₂: An antiferromagnetic local-moment metal, *Phys. Rev. Lett.* **108**, 087005 (2012), URL <https://doi.org/10.1103/PhysRevLett.108.087005>.
- ⁵⁶ J. Lamsal, G. S. Tucker, T. W. Heitmann, A. Kreyssig, A. Jesche, A. Pandey, W. Tian, R. J. McQueeney, D. C. Johnston, and A. I. Goldman, Persistence of local-moment antiferromagnetic order in Ba_{1-x}K_xMn₂As₂, *Phys. Rev. B* **87**, 144418 (2013), URL <https://doi.org/10.1103/PhysRevB.87.144418>.
- ⁵⁷ G. S. Tucker, D. K. Pratt, M. G. Kim, S. Ran, A. Thaler, G. E. Granroth, K. Marty, W. Tian, J. L. Zarestky, M. D. Lumsden, S. L. Bud'ko, P. C. Canfield, A. Kreyssig, A. I. Goldman, and R. J. McQueeney, Competition between stripe and checkerboard magnetic instabilities in Mn-doped BaFe₂As₂, *Phys. Rev. B* **86**, 020503(R) (2012), URL <https://doi.org/10.1103/PhysRevB.86.020503>.
- ⁵⁸ A. Pandey, V. K. Anand, and D. C. Johnston, Large miscibility gap in the Ba(Mn_xFe_{1-x})₂As₂ system, *Phys. Rev. B* **84**, 014405 (2011), URL <https://doi.org/10.1103/PhysRevB.84.014405>.
- ⁵⁹ S. Medvedev et al., unpublished.